A Rate-Dependent, Elasto-Plastic Cohesive Zone Mixed-Mode Model for Crash Analysis of Adhesively Bonded Joints

Stephan Marzi[1], Olaf Hesebeck[1], Markus Brede[1], Felix Kleiner[2]
[1]Fraunhofer IFAM, Bremen, Germany
[2]Henkel AG & Co. KGaA, Garching, Germany

© Copyright by DYNAmore

Summary:

Presently, there are various cohesive zone models implemented in LS-DYNA. The simplest one consists of a bi-linear traction separation-law in both modes I and II. Further models allow more complicated shapes of the traction-separation law, such as the material model of Tvergaard and Hutchinson or the General Cohesive Zone Model. However, none of these implemented models consider rate-dependency or effects of plasticity.

Crash-optimized structural adhesives used in automotive structures, as for example Henkel Terokal 5077, often show a rate-dependent elastic-plastic material behaviour. An extended mixed-mode cohesive zone model is proposed in this paper. The model considers the effects of rate-dependency and plasticity, and therefore is able to predict the failure of adhesively bonded joints more precisely than the common models. The material parameters describing the rate-dependency of yield strengths or critical energy release rates can be identified directly by (fracture) mechanical tests.

The new model is validated by simulations of single lap-shear, T-peel, End-Loaded Shear Joint (ELSJ) and Tapered Double Cantilever Beam (TDCB) tests. A comparison of numerical and experimental results shows the benefits and the limitations of the new model, which will be available from one of the next versions of LS-DYNA. Its official name will be MAT_COHESIVE_MIXED_MODE_ELASTOPLASTIC_RATEDEPENDENT, or in short MAT_240. The tests were proceeded at velocities ranging over several orders of magnitude. The results, which depend strongly on the test velocity, are predicted well by the new model. Further advantages are seen, when simulating a specimen unloading during a TDCB test. The irreversible displacement after unloading, which is caused by the adhesive's plasticity, is obtained also in simulations when using the new model.

Finally, a side-impact test on a floor pan is simulated, using the new model to predict the failure of adhesive bond lines connecting a cross beam to the structure. The crash tests were performed by Adam Opel GmbH. First simulations of such impact tests, using MAT_138 to model the adhesive layer, were already presented at the recent German LS-DYNA-Forum in Bamberg. The new results obtained with the elastic-plastic, rate-dependent MAT_240 show a good agreement with the experimentally observed behaviour. Thus, the model has been successfully employed in the crash simulation of a large, bonded vehicle structure.

Keywords:

crash analysis, cohesive zone model, structural adhesive bonding, mixed-mode, rate-dependency, fracture mechanics, plasticity

© 2009 Copyright by DYNAmore GmbH

1 MAT_240 Model Description

The MAT_240 is a tri-linear elastic-ideally plastic cohesive zone model. Its traction-separation law looks similar to MAT_185 [1], but it further considers effects of plasticity and rate-dependency. A similar tri-linear shape of the traction-separation law is also used by De Moura et al. [2], but the authors neither describe the plastical material behaviour nor its rate-dependency. In the model proposed here, the entire separation at failure is plastic, no brittle fracture behaviour can be modelled with this material type.

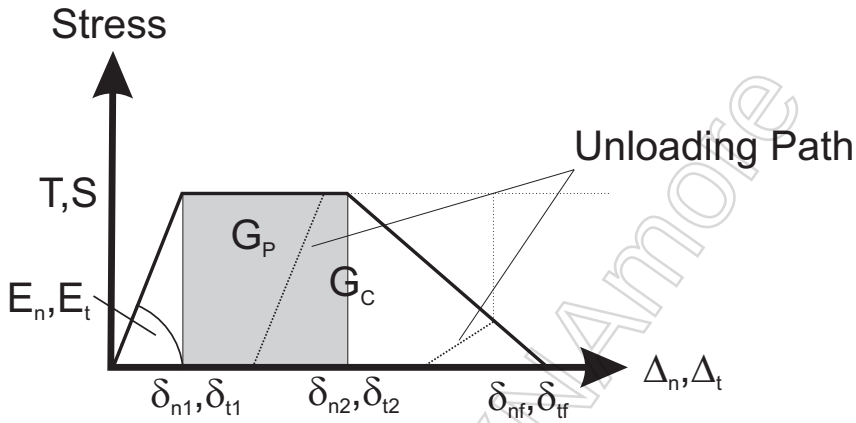

Figure 1: Tri-linear traction-separation law

The separations Δ_n in normal (peel) and Δ_t in tangential (shear) direction are calculated from the element's separations in the integration points,

$$\Delta_n = \langle u_n \rangle \text{ and } \Delta_t = \sqrt{u_{t1}^2 + u_{t2}^2},\ \langle x \rangle = \begin{cases} x, & \text{if } x > 0 \\ 0, & \text{else} \end{cases} \tag{1}$$

u_n, u_{t1} and u_{t2} are the separations in normal and in the both tangential directions of the element coordinate system. The total (mixed-mode) separation Δ_m is determined by

$$\Delta_m = \sqrt{\Delta_n^2 + \Delta_t^2}. \tag{2}$$

The initial stiffnesses E_n and E_t in both modes are calculated from the elastic Young's modulus E and the shear modulus G, $E_n = \frac{E}{t_{elem}}$ and $E_t = \frac{G}{t_{elem}}$, where t_{elem} , the element's thickness, is an user defined value, which can also be obtained as distance between the initial positions of the element's corner nodes (Nodes 1-5, 2-6, 3-7 and 4-8, respectively).

When the total energy under the traction-separation law is given by G_C, one further parameter is needed to describe the exact shape of the tri-linear material model. If the energy under the constant stress (plateau) region is denoted G_P (figure 1), a parameter f_{Gi} $(i = 1,2)$ defines the shape of the traction-separation law,

$$0 \leq f_{G1} = \frac{G_{IP}}{G_{IC}} < 1 - \frac{T^2}{2G_{IC}E_n} < 1 \tag{3}$$

$$0 \leq f_{G2} = \frac{G_{IIP}}{G_{IIC}} < 1 - \frac{S^2}{2G_{IIC}E_t} < 1 \tag{4}$$

for mode I and mode II loading, respectively.

Copyright by DYNAmore

While f_{G1} and f_{G2} are always constant values, T, S, G_{IC} and G_{IIC} may be chosen as functions of an equivalent strain rate $\dot{\varepsilon}_{eq}$, which is evaluated by

$$\dot{\varepsilon}_{eq} = \frac{\sqrt{\dot{u}_n^2 + \dot{u}_{t1}^2 + \dot{u}_{t2}^2}}{t_{elem}}. \tag{5}$$

$\dot{u}_n, \dot{u}_{t1}$ and $\dot{u}_{t2}$ represent the velocities corresponding to the separations u_n, u_{t1} and u_{t2}.

For the yield stresses T under tension and S under shear, two rate-dependent and one rate-independent formulations are implemented for each mode:

1. A quadratic logarithmic function:

$$T\left(\dot{\varepsilon}_{eq}\right) = T_0 + T_1 \langle \ln \frac{\dot{\varepsilon}_{eq}}{\dot{\varepsilon}_T} \rangle^2 \tag{6}$$

$$S\left(\dot{\varepsilon}_{eq}\right) = S_0 + S_1 \langle \ln \frac{\dot{\varepsilon}_{eq}}{\dot{\varepsilon}_S} \rangle^2 \tag{7}$$

2. A linear logarithmic function:

$$T\left(\dot{\varepsilon}_{eq}\right) = T_0 + T_1 \langle \ln \frac{\dot{\varepsilon}_{eq}}{\dot{\varepsilon}_T} \rangle \tag{8}$$

$$S\left(\dot{\varepsilon}_{eq}\right) = S_0 + S_1 \langle \ln \frac{\dot{\varepsilon}_{eq}}{\dot{\varepsilon}_S} \rangle \tag{9}$$

3. Alternatively, T and S can be chosen as constant values.

$$T\left(\dot{\varepsilon}_{eq}\right) = T_0 \tag{10}$$

$$S\left(\dot{\varepsilon}_{eq}\right) = S_0 \tag{11}$$

The rate-dependency of the fracture energies are given by

$$G_{IC}\left(\dot{\varepsilon}_{eq}\right) = G_{I0} + \left(G_{I\infty} - G_{I0}\right) \exp\left(-\frac{\dot{\varepsilon}_{G1}}{\dot{\varepsilon}_{eq}}\right), \tag{12}$$

$$G_{IIC}\left(\dot{\varepsilon}_{eq}\right) = G_{II0} + \left(G_{II\infty} - G_{II0}\right) \exp\left(-\frac{\dot{\varepsilon}_{G2}}{\dot{\varepsilon}_{eq}}\right). \tag{13}$$

Also for the critical energy release rates, constant values may be defined by the user,

$$G_{IC}\left(\dot{\varepsilon}_{eq}\right) = G_{I0}, \tag{14}$$

$$G_{IIC}\left(\dot{\varepsilon}_{eq}\right) = G_{II0}. \tag{15}$$

It should be noticed, that the equivalent strain rate $\dot{\varepsilon}_{eq}$ is updated until the yield initiation criterion $\Delta_m > \delta_{m1}$ is satisfied. When $\Delta_m > \delta_{m1}$, the model behaviour depends on the equivalent strain rate at yield initiation. Further information on the implemented rate-dependencies can be found in [3, 4].

Copyright by DYNAmore

Having defined the parameters describing the single modes, the mixed-mode behaviour is formulated by quadratic initiation criteria for both yield stress and damage initiation, while the damage evolution follows a Power-Law.

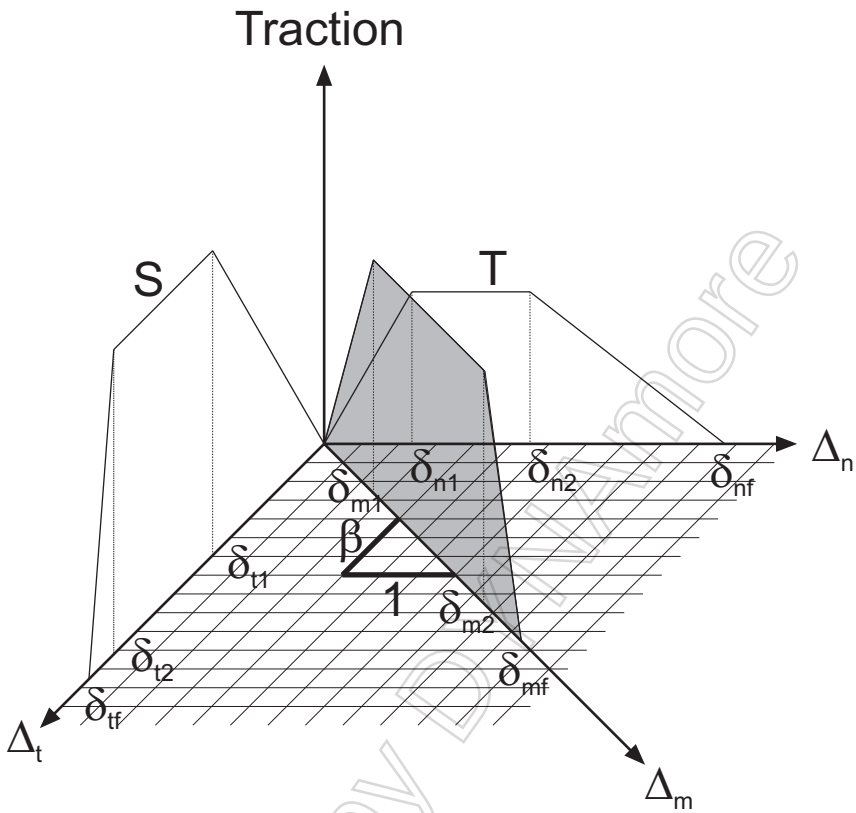

Figure 2: Tri-linear, mixed-mode traction-separation law

The mixed-mode yield initiation displacement δ_{m1} is defined as

$$\delta_{m1} = \delta_{n1}\delta_{t1}\sqrt{\frac{1+\beta^2}{\delta_{t1}^2 + (\beta\,\delta_{n1})^2}}, \tag{16}$$

$\delta_{n1} = \frac{T}{E_n}$ and $\delta_{t1} = \frac{S}{E_t}$ represent the single-mode yield initiation displacements and $\beta = \frac{\delta_{t1}}{\delta_{n1}}$ is the mixed-mode ratio.

Similar to the yield initiation, the damage initiation displacement is defined as:

$$\delta_{m2} = \delta_{n2}\delta_{t2}\sqrt{\frac{1+\beta^2}{\delta_{t2}^2 + (\beta\,\delta_{n2})^2}}, \tag{17}$$

with $\delta_{n2} = \delta_{n1} + \frac{f_{G1}G_{IC}}{T}$ and $\delta_{t2} = \delta_{t1} + \frac{f_{G2}G_{IIC}}{S}$.

With $\gamma = \arccos\frac{\langle u_n\rangle}{\Delta_m}$, the ultimate (failure) displacement δ_{mf} can be written,

$$\delta_{mf} = \frac{\delta_{m1}\left(\delta_{m1}-\delta_{m2}\right)E_nG_{IIC}\cos^2\gamma + G_{IC}\left(2G_{IIC} + \delta_{m1}\left(\delta_{m1}-\delta_{m2}\right)E_t\sin^2\gamma\right)}{\delta_{m1}\left(E_nG_{IIC}\cos^2\gamma + E_tG_{IC}\sin^2\gamma\right)}. \tag{18}$$

This formulation describes a power-law damage evolution with an exponent $\eta = 1.0$ (in comparison with MAT_138).

After the shape of the mixed-mode traction-separation law has been determined by δ_{m1}, δ_{m2} and δ_{mf}, the plastic separations $u_{n,P}, u_{t1,P}$ and $u_{t2,P}$ can be calculated in each element direction. The plastic separation in peel direction is given by

© 2009 Copyright by DYNAmore GmbH

$$u_{n,P} = max\left(u_{n,P,t_{i-1}}, u_n - \delta_{m1}\sin\gamma, 0\right), \tag{19}$$

t_{i-1} indicates the individual value from the last time increment.

In the shear direction, an elastic shear separation $\delta_{t,y}$,

$$\delta_{t,y} = \sqrt{\left(u_{t1} - u_{t1,P,t_{i-1}}\right)^2 + \left(u_{t1} - u_{t1,P,t_{i-1}}\right)^2} \tag{20}$$

is defined. If $\delta_{t,y} > \delta_{m1}\sin\gamma$, the plastic shear separations in the element coordinate system are updated,

$$u_{t1,P} = u_{t1,P,t_{i-1}} + u_{t1} - u_{t1,t_{i-1}}, \text{ and} \tag{21}$$

$$u_{t2,P} = u_{t2,P,t_{i-1}} + u_{t2} - u_{t2,t_{i-1}}. \tag{22}$$

In case $\Delta_m > \delta_{m2}$, the damage initiation criterion is satisfied and a damage variable D increases monotonically,

$$D = max\left(\frac{\Delta_m - \delta_{m2}}{\delta_{mf} - \delta_{m2}}, D_{t_{i-1}}, 0\right). \tag{23}$$

When $\Delta_m > \delta_{mf}$, complete damage ($D = 1$) is reached and the element fails in the corresponding integration point.

Finally, the peel and the shear stresses in element directions are calculated, but no damage under pressure loads is considered in peel direction.

$$\sigma_{t1} = E_t\left(1 - D\right)\left(u_{t1} - u_{t1,P}\right), \tag{24}$$

$$\sigma_{t2} = E_t\left(1 - D\right)\left(u_{t2} - u_{t2,P}\right), \text{ and} \tag{25}$$

$$\sigma_n = \begin{cases} E_n\left(1 - D\right)\left(u_n - u_{n,P}\right), & \text{if } u_n - u_{n,P} > 0 \\ E_n\left(u_n - u_{n,P}\right), & \text{else.} \end{cases} \tag{26}$$

2 Model Validation

The MAT_240 is validated by comparison of several coupon tests at different load rates with numerical predictions. Single lap-shear, T-peel and Tapered Double Cantilever Beam tests are performed at velocities ranging over five orders of magnitude. The simulation of an End-Loaded Shear Joint test shows the benefits of MAT_240 compared with the bi-linear, rate-independent MAT_138. All experiments were proceeded with the crash-optimized adhesive Henkel Terokal 5077.

2.1 Tapered Double Cantilever Beam (TDCB) tests

TDCB tests were simulated at three different test velocities. In the simulations as in the experiments, the crack propagation through the adhesive layer is stopped by unloading of the specimen. Due to the plasticity of the adhesive, an offset-displacement is observed when the specimen is completely unloaded. MAT_240 is able to predict this offset-displacement sufficiently (figures 3 to 5).

Copyright by DYNAmore

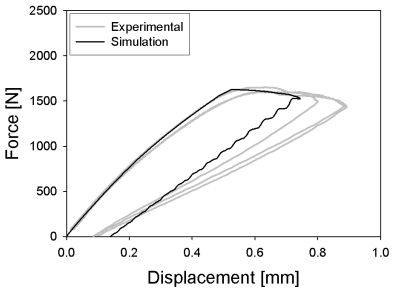

Figure 3: TDCB tests, experimental and simulation, $v_{test} = 6 \times 10^{-4}\,\mathrm{mm/s}$

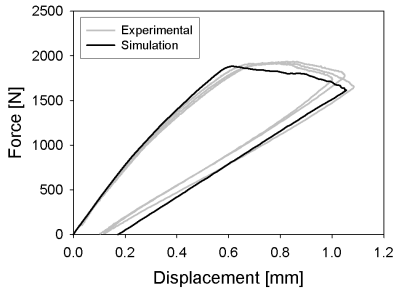

Figure 4: TDCB tests, experimental and simulation, $v_{test} = 1.7 \times 10^{-1}\,\mathrm{mm/s}$

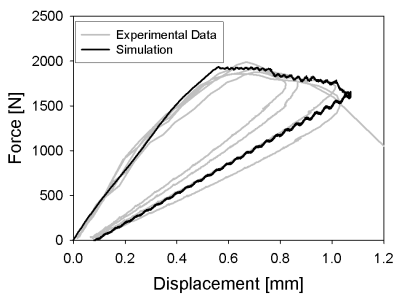

Figure 5: TDCB tests, experimental and simulation, $v_{test} = 170\,\mathrm{mm/s}$

2.2 T-peel tests

T-peel tests were proceeded at three velocities for three combinations of adherent steel sheets. Samples, manufactured from two steel adherends with thickness $t_{steel} = 1.4\,\mathrm{mm}$, were tested at $v_{test} = 3\,\mathrm{mm/s}$ (figure 6) and $v_{test} = 100\,\mathrm{mm/s}$ (figure 7). Two further adherend combinations were tested in a rotary impact device with an impact velocity $v_{test} = 5000\,\mathrm{mm/s}$ (figures 8 and 9). All experimental data fit well to the numerically obtained results (at high test velocities, the numerical curves are smoothed for readability only).

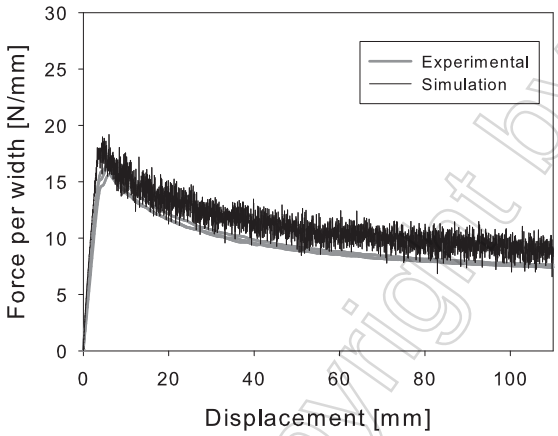

Figure 6: T-peel tests, $v_{test} = 3\,\mathrm{mm/s}$, two steel adherends, $t_{steel} = 1.4\,\mathrm{mm}$

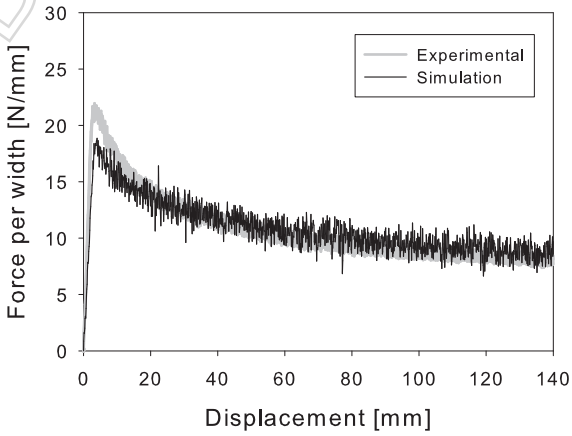

Figure 7: T-peel tests, $v_{test} = 100\,\mathrm{mm/s}$, two steel adherends, $t_{steel} = 1.4\,\mathrm{mm}$

Copyright by DYNAmore

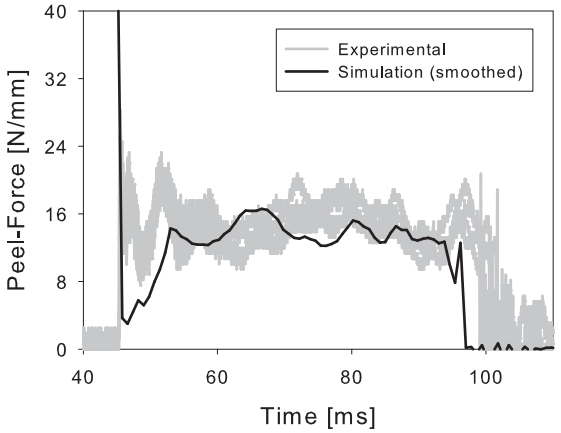

Figure 8: T-peel tests, $v_{test} = 5000\,\mathrm{mm/s}$, two steel adherends, $t_{steel} = 0.8\,\mathrm{mm}$

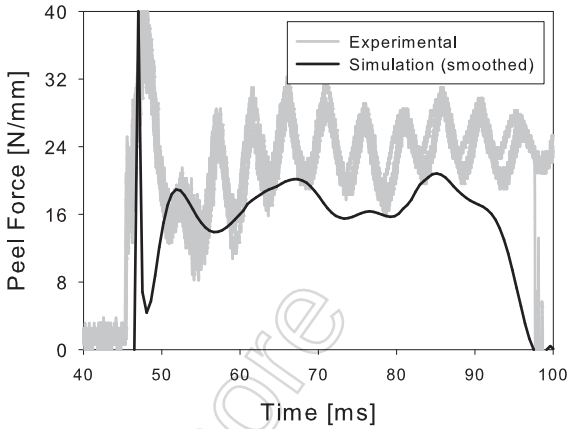

Figure 9: T-peel tests, $v_{test} = 5000\,\mathrm{mm/s}$, $t_{steel,1} = 0.8\,\mathrm{mm}$ and $t_{steel,2} = 1.4\,\mathrm{mm}$

2.3 Single lap-shear tests

Similar to the T-peel tests, simulations of single lap-shear tests were performed for different load rates and different adherend combinations. The figures 10 to 12 show examples of the comparison of numerical and experimental data.

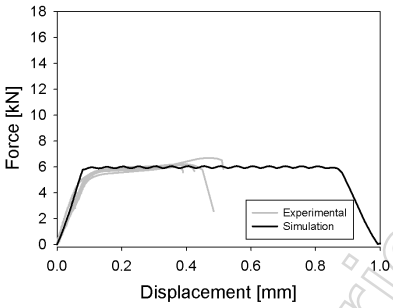

Figure 10: Single lap-shear tests, $v_{test} = 0.01\,\mathrm{mm/s}$

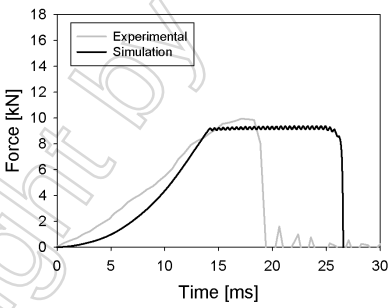

Figure 11: Single lap-shear tests, $v_{test} = 100\,\mathrm{mm/s}$

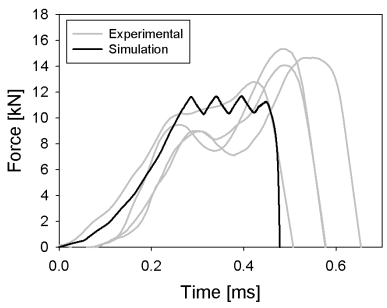

Figure 12: Singe Lap-Shear tests, $v_{test} = 5000\,\mathrm{mm/s}$

The plateau force seen in the tests is reached also in the simulations. In figures 10 and 11, the adhesive joint fails earlier than predicted by the numerical model. This earlier failure is mainly caused by a partly adhesive failure of the adhesive layer. Such adhesive failure can not be described by the material model, since its parameter identification is restricted to cohesive failure inside the adhesive bulk. At the crash-relevant high speeds tests (figure 12), conducted in a rotary impact device, purely cohesive failure is detected. In this case, simulation and experimental results agree well.

2.4 End-Loaded Shear Joint (ELSJ) specimen

The End-Loaded Shear Joint (ELSJ) specimen (fig. 14) is a recently developed specimen type, which can be used to measure the critical energy release rate, G_{IIC}, for adhesively bonded joints loaded in shear as proposed in [4]. Figure 13 shows a comparison of simulation results of such ELSJ test, using both MAT_240 and MAT_138, with experimental data. The material parameters for the MAT_138 were chosen, so that the traction-separation-law agrees with the one resulting from $f_{g,i} = 0.0$ in the MAT_240. In contrast to the tests, no unloading was considered in the simulations. It is seen, that MAT_138 predicts

Copyright by DYNAmore

an earlier failure than it is noticed in the experiment, while the results of MAT_240 agree very well with the experimental one.

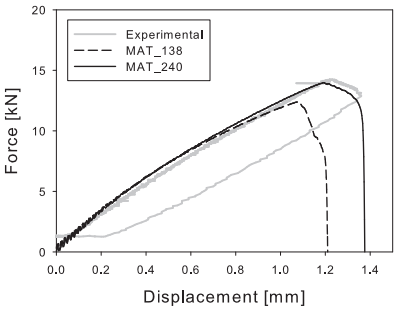

Figure 13: Comparison of simulation results of an ELSJ test, using MAT_240 and MAT_138, to experimental data

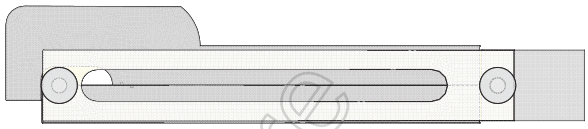

Figure 14: Finite element model of an End-Loaded Shear Joint (ELSJ) specimen

3 Application in a simulation of a large, bonded vehicle structure

In the recent German LS-DYNA-Forum in Bamberg, investigations about the usage of cohesive elements in large, bonded vehicle structures were presented [5]. Side crash tests were performed on a vehicle floor pan by Adam Opel GmbH (figure 15), the test results were compared with numerical results, the adhesive layer was modelled using MAT_138. This paper presents further variants of these tests and further simulations with MAT_240. Detailed information on the test setup and the numerical model can be found in [5].

Figure 15: Floor pan, specimen with test setup and numerical model with locations of acceleration sensors

In summary, three further variants were tested by OPEL:

- The cross beam is bonded with Henkel Terokal 5077 to the remaining structure. The fixing spot welds were removed after adhesive hardening to avoid their influences in the simulation.
- The cross beam is connected with Henkel Terokal 5077 and 10 additional spot weld points to the remaining structure.
- The cross beam is spot welded at 11 points to the structure without adhesive.

© 2009 Copyright by DYNAmore GmbH

For these three tested variants, experimental results are shown in figures 16 and 17 for two sensor locations (see figure 15). The plotted velocities and displacements are obtained by integrating the measured accelerations. Two specimens were tested for each variant.

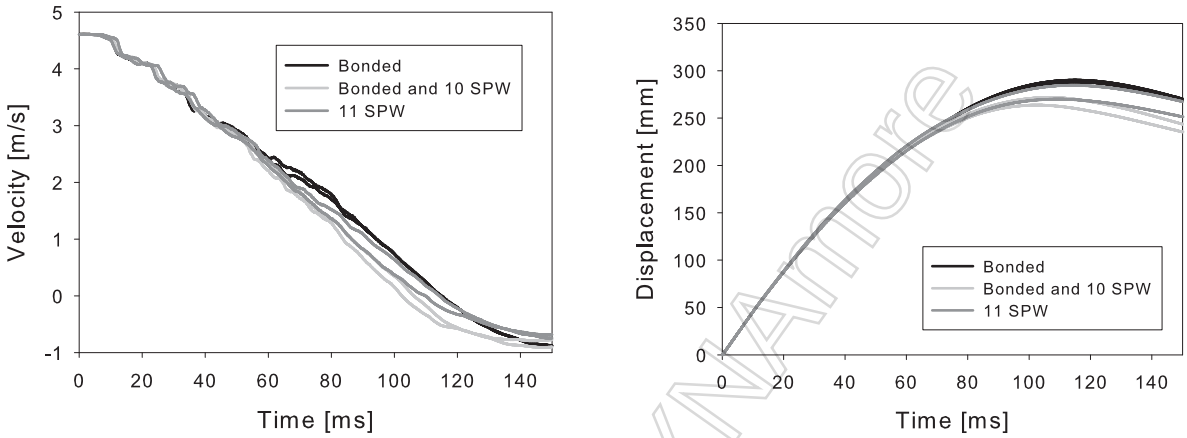

Figure 16: Impact tests on floor pan, measurement on dolly (impact direction)

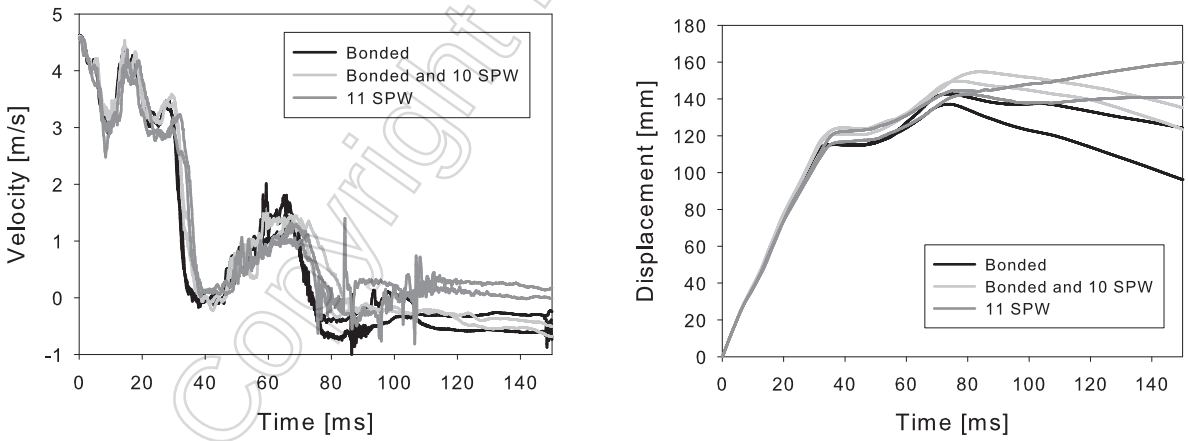

Figure 17: Impact tests on floor pan, measurement on flange of cross beam (impact direction)

The results of the three variants differ slightly. However, the combination of adhesive bonding with spot welding leads the smallest impact displacement (see figure 16, right), while the bonded variants show no significant differences to the spot welded ones. The comparison of experimental data with numerical predictions for the locations mentioned above is shown in figures 18 and 19 for the bonded variant. For the other two variants no simulation results are presently available.

Copyright by DYNAmore

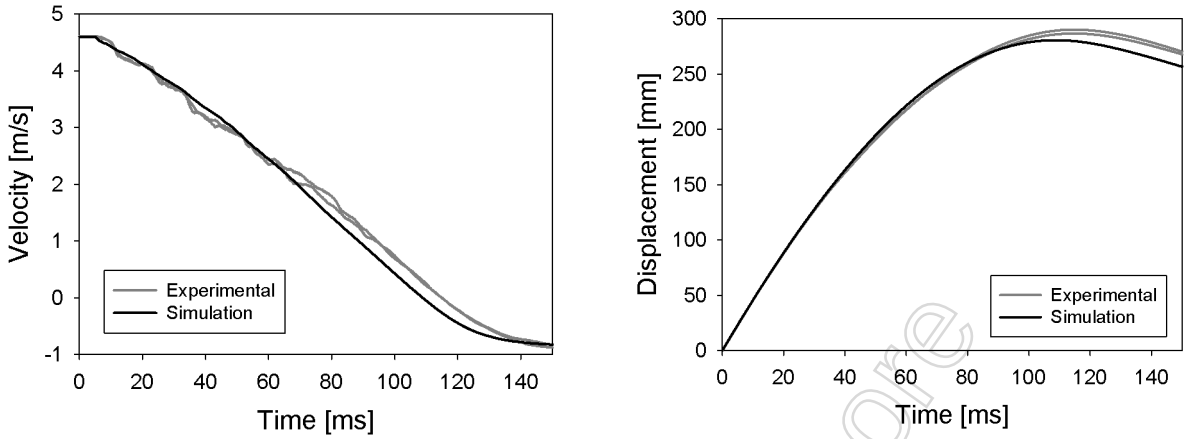

Figure 18: Bonded variant, measurement on dolly (impact direction), experimental and simulation

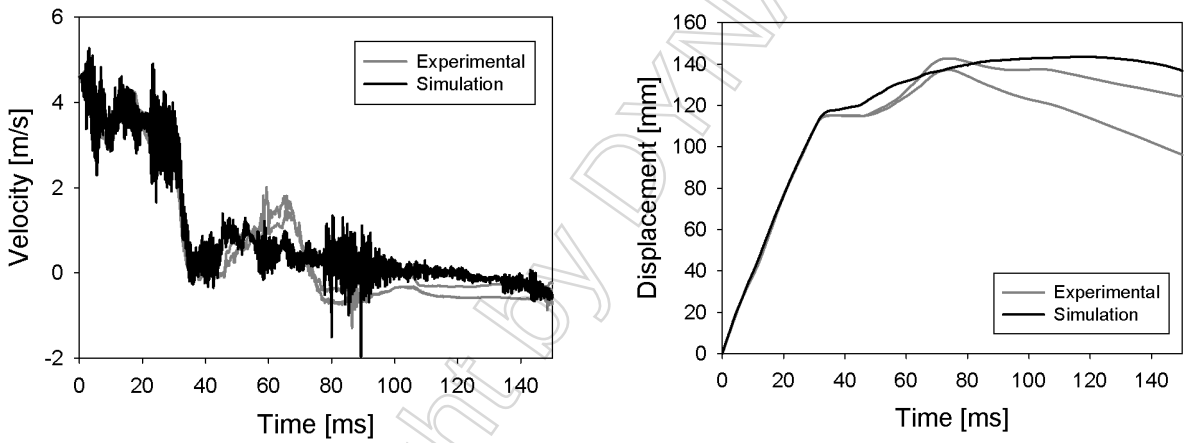

Figure 19: Bonded variant, measurement on flange of cross beam (impact direction), experimental and simulation

Finally the folding of the floor pan at $t = 150\,\mathrm{ms}$ after impact is given in figure 20. Only small deviations between simulation and test are obtained. Thus, the elastic-plastic, rate-dependent MAT_240 was successfully applied in a large, bonded vehicle structure.

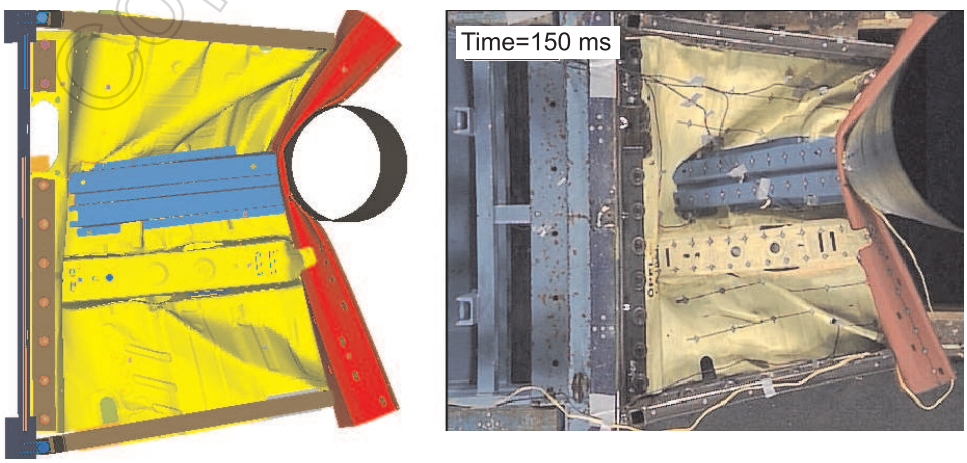

Figure 20: Folding of floor pan at impact time $t = 150\,\mathrm{ms}$

Copyright by DYNAmore

Acknowledgement The authors would like to acknowledge the contributions from Laia Ramon-Villalonga and Mathias Poklitar (Adam Opel GmbH) to this paper.

4 Literature

[1] Livermore Software Technology Corporation. *LS-DYNA Keyword User's Manual, Volume I, Version 971*. 7374 Las Pas Road, Livermore, CA 94551, May 2007. ISBN 0-9778540-2-7.

[2] M.F.S.F. De Moura, J.P.M. Goncalves, J.A.G. Chousal, and R.D.S.G. Campilho. Cohesive and continuum mixed-mode damage models applied to the simulation of the mechanical behaviour of bonded joints. *Int. J. Adhesion Adhesives*, 28:419–426, 2008.

[3] S. Marzi, O. Hesebeck, M. Brede, and F. Kleiner. A rate-dependent cohesive zone model for adhesive layers loaded in mode I. *J. Adh. Sc. Tech.*, 23:881–898, 2009.

[4] S. Marzi, O. Hesebeck, M. Brede, and F. Kleiner. An end-loaded shear joint (ELSJ) specimen to measure the critical energy release rate of tough, structural adhesives in mode II. *J. Adh. Sc. Tech.*, 2009. submitted for publication.

[5] S. Marzi, L. Ramon-Villalonga, M. Poklitar, and F. Kleiner. Usage of cohesive elements in crash analysis of large, bonded vehicle structures - experimental tests and simulation. In *German LS-Dyna Forum Bamberg*, pages B.I.1–B.I.19, 2008.

Copyright by DYNAmore

© 2009 Copyright by DYNAmore GmbH